Journal of Magnetic Resonance 206 (2010) 105–111

Contents lists available at ScienceDirect

Journal of Magnetic Resonance

journal homepage: www.elsevier.com/locate/jmr

# $^{1}H$–$^{13}C$ separated local field spectroscopy of uniformly $^{13}C$ labeled peptides and proteins

Eugene C. Lin, Chin H. Wu, Yuan Yang, Christopher V. Grant, Stanley J. Opella *

*Department of Chemistry and Biochemistry, University of California San Diego, 9500 Gilman Drive, La Jolla, CA 92093-0307, United States*

ARTICLE INFO

*Article history:*
Received 19 May 2010
Revised 22 June 2010
Available online 1 July 2010

*Keywords:*
$^{13}C$ NMR
PISEMO
Solid-state NMR
Oriented samples

ABSTRACT

By incorporating homonuclear decoupling on both the $^{1}H$ and $^{13}C$ channels it is feasible to obtain high-resolution two-dimensional separated local field spectra of peptides and proteins that are 100% labeled with $^{13}C$. Dual-PISEMO (Polarization Inversion Spin Exchange Modulated Observation) can be performed as a conventional two-dimensional experiment, or with windowed detection as a one-dimensional experiment that offers flexibility as a building block for shiftless and other multidimensional triple-resonance experiments with the inclusion of $^{15}N$ irradiation. The triple-resonance MAGC probe used to perform these experiments at 500 MHz is described.



## 1. Introduction

Extending the scope of uniform labeling with $^{15}N$ from molecular biology [1] to NMR spectroscopy [2] opened up many opportunities for structural studies of biopolymers. The further extension of uniform labeling to include both $^{13}C$ and $^{15}N$ has led to the wide spread implementation of triple-resonance $^{1}H/^{13}C/^{15}N$ experiments in solution-state NMR [3] and in magic angle spinning (MAS) solid-state NMR [4] of proteins. In contrast, there have been few applications of $^{1}H/^{13}C/^{15}N$ triple-resonance experiments to stationary solid samples, single crystals, or uniaxially aligned samples [5]. The principal reason is that the tight network of $^{13}C$–$^{13}C$ homonuclear dipole–dipole couplings in molecules where all carbon sites are 100% labeled with $^{13}C$ interferes with most solid-state NMR experiments, including the direct detection of single-line $^{13}C$ resonances and the evolution of $^{1}H$–$^{13}C$ dipolar couplings in various separated local field (SLF) experiments [6]. These couplings undoubtedly interfere with a wide variety of other experiments.

We have made some progress in developing triple-resonance experiments for stationary samples by implementing homonuclear $^{13}C$–$^{13}C$ decoupling in indirect dimensions [7] and through the use of tailored $^{13}C$ labeling [8] to minimize the number of directly bonded pairs of $^{13}C$ nuclei with strong homonuclear dipole–dipole couplings. In this article we describe further development of $^{1}H/^{13}C/^{15}N$ triple-resonance experiments for solid-state NMR of stationary samples that involves the use of pulse sequences that integrate homonuclear $^{13}C$–$^{13}C$ decoupling into the previously described Polarization Inversion Spin Exchange Modulated Observation (PISEMO) version [9] of SLF experiments. By simultaneously employing both $^{1}H$–$^{1}H$ and $^{13}C$–$^{13}C$ homonuclear decoupling in the pulse sequence, experiments can be performed on 100% uniformly $^{13}C$ labeled samples. Further, these experiments have the option of enabling the $^{13}C$ magnetization to be detected in the windows of the multiple-pulse cycle, reducing the dimensionality and serving as an essential building block for Shiftless NMR experiments where heteronuclear dipolar couplings provide all of the frequency dimensions [10].

The dipole–dipole couplings between two nuclei are manifested as doublets in solid-state NMR spectra. $^{1}H$–$^{13}C$ dipolar couplings can be measured directly when they are spatially isolated and interactions in the lattice are negligible [11]. Heteronuclear dipolar couplings can be observed when homonuclear decoupling procedures [12,13] are applied to the abundant spins. In general, the abundant spin referred to is $^{1}H$; however, $^{13}C$ can also be considered an abundant spin in 100% uniformly $^{13}C$ labeled samples. Pulse sequences that perform homonuclear decoupling without removing the chemical shift or heteronuclear dipolar interactions are of particular interest for structural studies, since the principles of selective averaging enable the measurement of structural constraints. SLF experiments in particular provide a powerful approach to obtaining distance and/or angular constraints for structure determination, since the heteronuclear dipole–dipole couplings associated with sites with resolved chemical shifts are measured [14]. For studies of proteins it is essential to use a high resolution version of SLF spectroscopy, such as Polarization Inversion Spin Exchange at the Magic Angle (PISEMA) [15], SAMPI4 [16], or PISEMO (Fig. 1A) [9] experiments because they provide narrow

* Corresponding author. Fax: +1 858 822 4821.
*E-mail address:* sopella@ucsd.edu (S.J. Opella).

1090-7807/$ - see front matter © 2010 Elsevier Inc. All rights reserved.
doi:10.1016/j.jmr.2010.06.011

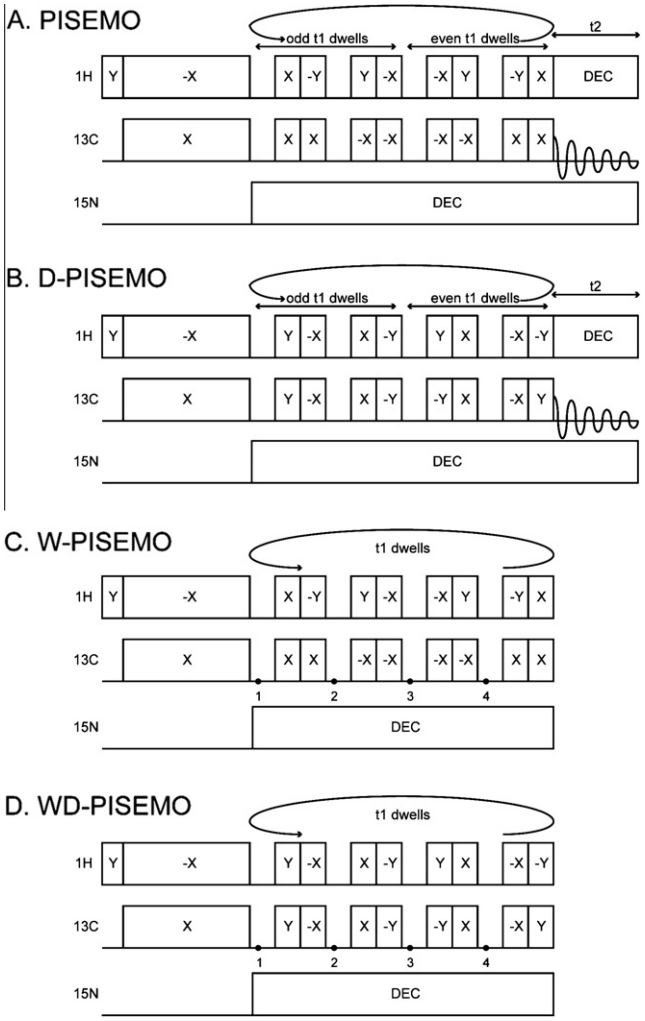


**Fig. 1.** Timing diagrams for pulse sequences. (A) $^{1}H/^{13}C$ (with $^{15}N$ decoupling) PISEMO. (B) $^{1}H/^{13}C$ (with $^{15}N$ decoupling) Dual-PISEMO. C. $^{1}H/^{13}C$ (with $^{15}N$ decoupling) Window-detected PISEMO. (D) $^{1}H/^{13}C$ (with $^{15}N$ decoupling) Window-detected Dual-PISEMO. CW refers to continuous wave irradiation. SPINAL-16 refers to modulated irradiation [21].

line widths in both the chemical shift and heteronuclear dipolar coupling frequency dimensions. The vast majority of applications of these experiments have focused on isolated $^{1}H–^{15}N$ amide and $^{1}H–^{13}C\alpha$ sites in the backbone of proteins where the heteronuclear dipolar couplings of these two-spin systems are observed as doublets; the pulse sequences perform homonuclear $^{1}H–^{1}H$ decoupling, and the homonuclear couplings among the 'dilute' $^{15}N$ or $^{13}C$ sites are negligible and can be ignored. Because the bond lengths are constant, the angular dependence of the frequency splittings between the doublets provides valuable input for structure determinations in oriented-sample (OS) solid-state NMR [17–19].

In order to integrate $^{1}H/^{13}C/^{15}N$ triple-resonance spectroscopy into OS solid-state NMR of 100% $^{13}C$ and $^{15}N$ labeled proteins, it is essential to deal with the $^{13}C–^{13}C$ homonuclear dipole–dipole couplings. $^{13}C$-detected versions of solid-state NMR experiments are of particular interest because of the potential for increased sensitivity over the more commonly employed $^{15}N$-detected experiments; we have observed a fourfold increase in sensitivity in directly comparable solid-state NMR experiments using the same sample and probe [8]. We are taking two distinct approaches in our studies of proteins. In one approach, tailored isotopic labeling [8] is employed, since this can provide samples where $^{13}C$ sites are not bonded to other $^{13}C$ nuclei, and hence do not have strong homonuclear dipole–dipole couplings. It has the advantage that it allows for direct $^{13}C$ detection. However, it has several disadvantages. With most metabolic labeling schemes based on incorporation of specifically $^{13}C$ labeled precursors, for example glycerol, multiple samples are required in order to obtain signals from all carbon sites in the protein, and the limited number of vicinal $^{13}C$ labeled sites reduces the opportunities for homonuclear correlation experiments. Experiments can be performed on samples with about 25% of the carbon sites randomly labeled with $^{13}C$, since on a statistical basis there are few pairs of $^{13}C$ bonded to each other in this situation, and all sites are equally represented in the spectra. However, not only does this suffer from an absence of vicinal $^{13}C$ labeled sites for making spectral correlations, but also, the overall dilution of the $^{13}C$ reduces the sensitivity to approximately one-fourth of what it would be if the same sites were 100% labeled with $^{13}C$. Since the increase in sensitivity from direct $^{13}C$ detection compared to $^{15}N$ detection is about fourfold under comparable conditions, the dilution effectively cancels out any gain in sensitivity from the direct $^{13}C$ detection. The second approach is to implement pulse sequences that incorporate $^{13}C–^{13}C$ homonuclear decoupling at critical evolution periods [7,9,10,20–22], and this is the subject of this article.

## 2. Results

The PISEMO pulse sequence diagrammed in Fig. 1A differs from the original version [9] in that each cycle has four windows, instead of two, on the $^{13}C$ channel. The additional windows enable direct $^{13}C$ detection of frequency oscillations due to the evolution of the $^{1}H–^{13}C$ dipolar couplings with high sensitivity without degrading the line widths of the signals in the dipolar coupling frequency dimension of the spectrum. Following conventional spin-lock Hartmann-Hahn matched cross-polarization transfer of magnetization from $^{1}H$ to $^{13}C$ in the preparation period [23], both the $^{1}H$ and $^{13}C$ magnetization are spin-locked by the radiofrequency pulses to allow heteronuclear magnetization exchange during the evolution period. On the $^{1}H$ channel, an eight-pulse cycle is applied, the first half of which is a four-pulse WaHuHa cycle ($X$, $-Y$, $Y$, $-X$) [12], and the second half is a phase inverted four-pulse WaHuHa cycle ($-X$, $Y$, $-Y$, $X$). This eight-pulse cycle can be viewed as a "flip-flop" WaHuHa cycle, analogous to the irradiations applied in PISEMA [15] or SAMPI4 [16]. We have obtained similar results using other eight-pulse cycles such as MREV8 [24] and HW8 [25]. In general, these experiments are limited to eight-pulse cycles because the cycle times of longer pulse sequences prohibit the measurement of the largest $^{1}H–^{13}C$ heteronuclear dipolar couplings present in stationary solid samples. The original PISEMO pulse sequence was designed for the situation most commonly encountered in studies of proteins, where $^{1}H$ is the only type of abundant spin present, and one or a few $^{1}H$ are strongly coupled to a single spatially isolated $^{13}C$ or $^{15}N$; as a result, only the effects of the multiple-pulse homonuclear decoupling sequence on the $^{1}H$ channel were taken into account in its design.

For spin systems with two different types of abundant spins coupled to each other, as in 100% uniformly $^{13}C$ labeled proteins, where both the $^{1}H$ and $^{13}C$ spins are regarded as abundant, it is essential to apply multiple-pulse sequences that perform homonuclear decoupling on both $^{1}H$ and $^{13}C$ channels. This is accomplished in the D-PISEMO pulse sequence diagrammed in Fig. 1B where the flip-flop WaHuHa sequence ($Y$, $-X$, $X$, $-Y$, $-Y$, $X$, $-X$, $Y$) is applied on the $^{13}C$ channel and MREV8 ($Y$, $-X$, $X$, $-Y$, $Y$, $X$, $-X$, $-Y$) is applied on the $^{1}H$ channel. Similar results can be obtained by applying the MREV8 cycle to the $^{13}C$ channel while applying the flip-flop WaHuHa cycle to the $^{1}H$ channel. Other combinations are also possible

although, in general we find that significant line narrowing cannot be achieved when the same multiple-pulse sequences are applied to both channels. The spectra shown in the figures were acquired using the pulse sequences diagrammed in Fig. 1. In all the experiments, continuous irradiation at the $^{15}$N frequency provides heteronuclear decoupling from both the $^{1}$H and $^{13}$C spins.

Comparisons among spectra obtained with the pulse sequences diagrammed in Fig. 1 demonstrate the critical features of D-PISEMO applied to 100% uniformly $^{13}$C labeled peptides and proteins. These pulse sequences can be used to detect $^{13}$C chemical shifts (Fig. 1B) in two-dimensional experiments, or $^{1}$H–$^{13}$C heteronuclear dipole–dipole couplings (Fig. 1D) in a one-dimensional version. Conventional single-contact spin-lock cross-polarization was used to obtain the $^{1}$H and $^{15}$N decoupled one-dimensional $^{13}$C NMR spectra in Fig. 2A and D. The spectrum in Fig. 2A consists of four single-line resonances, one from each unique site in the unit cell of a single crystal where there is only one $^{13}$C labeled site in each molecule of the model peptide $^{15}$N, $^{13}$Cα N-acetyl-leucine (NAL). In contrast, the spectrum shown in Fig. 2D, which was obtained from a 100% uniformly $^{13}$C labeled single crystal of the model peptide N-acetyl-valine (NAV), is poorly resolved with broad, overlapping resonance intensity due to the effects of the homonuclear $^{13}$C–$^{13}$C dipole–dipole couplings. By itself, the comparison between the one-dimensional spectra in Fig. 2A and D demonstrates why it is essential to incorporate homonuclear $^{13}$C–$^{13}$C decoupling into experiments that are to be applied to 100% uniformly $^{13}$C labeled stationary samples.

Homonuclear decoupling in solids is generally accomplished with either multiple-pulse sequences, such as WaHuHa [12], or continuous off-resonance (Lee-Goldburg) irradiation [13]. Previously, we demonstrated that resonances with different $^{13}$C chemical shifts could be resolved in samples by applying $^{13}$C–$^{13}$C homonuclear decoupling in the indirect dimension of experiments performed with direct $^{15}$N detection [7], since only heteronuclear $^{1}$H and $^{13}$C decoupling is required during data acquisition to obtain high resolution spectra with single-line resonances. However, our goal is to utilize direct $^{13}$C detection in order to gain sensitivity and flexibility in experimental design, and this requires the use of homonuclear decoupling during data acquisition in order to obtain high-resolution $^{13}$C NMR spectra. Moreover, the same $^{13}$C–$^{13}$C homonuclear couplings that result in poor spectral resolution, as in Fig. 2D, interfere with the evolution of $^{1}$H–$^{13}$C heteronuclear dipolar couplings in SLF experiments performed on samples that are 100% uniformly labeled with $^{13}$C [26].

PISEMO yields two-dimensional SLF spectra with resolution and sensitivity similar to those obtained using the original PISEMA experiment with the added benefit of increased bandwidth, which is a significant advantage for experiments performed at high fields. We have shown that PISEMO can be performed with either direct $^{13}$C detection as a two-dimensional experiment, or with indirect $^{1}$H detection as a one-dimensional experiment, depending on whether the observation windows in the multiple-pulse sequence are used to detect the magnetization as it is transferred in an oscillatory manner between the $^{1}$H and $^{13}$C nuclei [9]. The frequencies of the oscillations are determined by the magnitudes of the individual heteronuclear $^{1}$H–$^{13}$C dipolar couplings. The D-PISEMO variant presented here effects both homonuclear $^{1}$H–$^{1}$H and homonuclear $^{13}$C–$^{13}$C decoupling during the heteronuclear

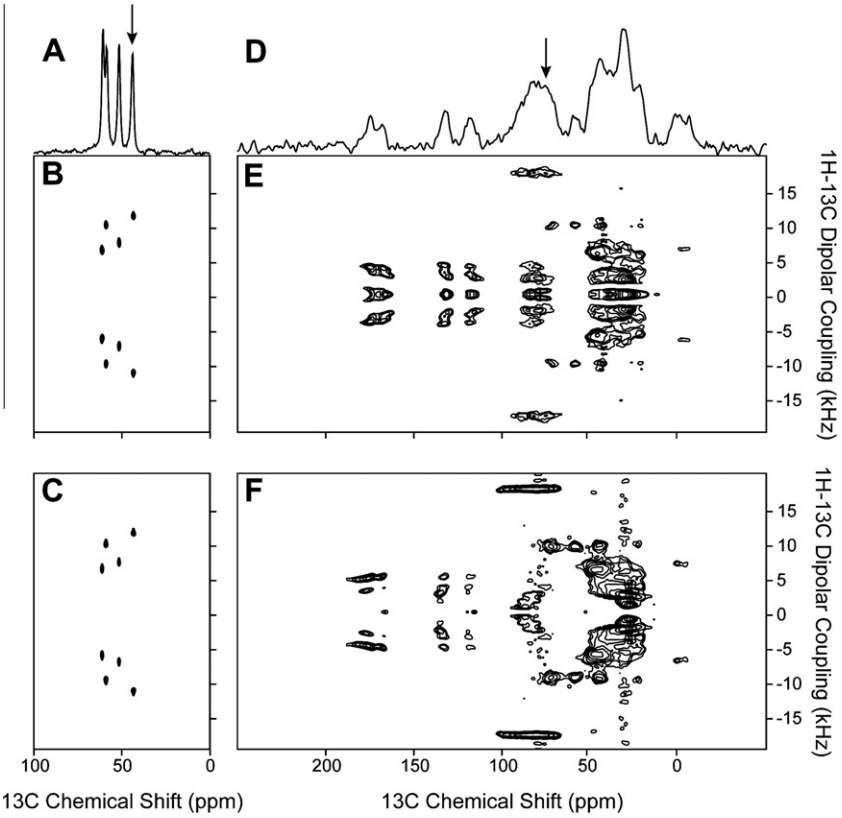


**Fig. 2.** $^{13}$C-detected solid-state NMR spectra. A–C were obtained from a $^{15}$N, $^{13}$Cα N-acetyl leucine (NAL) single crystal. D–F were obtained from a 100% uniformly $^{15}$N, $^{13}$C labeled N-acetyl valine (NAV) single crystal. (A) One-dimensional $^{1}$H and $^{15}$N decoupled $^{13}$C NMR spectrum obtained by cross-polarization. (B and E) Two-dimensional PISEMO spectra. (C and F) Two-dimensional D-PISEMO spectrum. The $^{1}$H carrier frequency was set at 4.7 ppm for all spectra; the $^{13}$C carrier frequency was set at 50 ppm for A–C. and at 100 ppm for D–F. All spectra were acquired with four scans, 64 $t_1$ points and 512 $t_2$ points. The dwell times were 36 μs and 20 μs for $t_1$ and $t_2$ dimensions respectively. The cross-polarization time was 1 ms and the recycle delay was 6 s. The experimental data were zero filled to 512 and 1024 data points in $t_1$ and $t_2$ dimensions and were multiplied by a sine bell window function prior to Fourier transformation.

$^{1}H$–$^{13}C$ spin-exchange period. $^{15}N$ heteronuclear decoupling is applied through continuous irradiation when necessary in molecules labeled with $^{15}N$ in addition to $^{13}C$. This enables D-PISEMO to be performed with direct $^{13}C$ detection in either a one- or two-dimensional experiment, considerably increasing its flexibility and potential applications in more complex multidimensional experiments.

The two-dimensional SLF spectra in Fig. 2B and C are very similar; they serve as controls to demonstrate the similarity of the performance of PISEMO and D-PISEMO for isolated $^{13}C$ sites unaffected by homonuclear $^{13}C$–$^{13}C$ dipole–dipole interactions. In both spectra, a doublet due to heteronuclear $^{1}H$–$^{13}C$ dipole–dipole coupling is associated with each resolved $^{13}C$ resonance in the one-dimensional chemical shift spectrum. The dipolar coupling spectra in Fig. 3A and B are associated with the $^{13}C\alpha$ resonance marked with an arrow in Fig. 2A. The frequencies of the signals, their line widths, and their intensities are essentially the same whether the spectra were obtained with the original version of PISEMO or D-PISEMO, demonstrating that for spatially isolated $^{13}C$ sites it is not necessary to apply homonuclear decoupling on the $^{13}C$ channel. In contrast, the situation is quite different for experiments performed on similar but 100% uniformly $^{13}C$ labeled samples. There are substantial differences between the spectra obtained with PISEMO (Figs. 2E and 3C) and D-PISEMO (Figs. 2F and 3D). Although it is somewhat difficult to visualize in the contour plots that include overlapping patterns from carbons bonded to between zero and three hydrogens, the PISEMO spectrum of a 100% uniformly $^{15}N$, $^{13}C$ labeled NAV single crystal (Fig. 2D) appears to be more complex with more spectral artifacts, especially for resonances with relatively small dipolar couplings than the corresponding D-PISEMO spectrum of the same sample (Fig. 2F). The arrow in Fig. 2D marks the frequency for a single $^{13}C\alpha$ resonance, as identified by analysis of individual spectral slices through the $^{1}H$–$^{13}C$ heteronuclear dipolar coupling dimension.

The spectral slices associated with the position of the arrow in Fig. 2D shown in Fig. 3C and D are dramatically different. Only with D-PISEMO is it possible to resolve and measure the splitting of the $^{1}H$–$^{13}C$ dipolar coupling doublet without distortions due to broadenings, splittings, and spectral artifacts emanating from the presence of the $^{13}C$–$^{13}C$ dipole–dipole couplings. The sensitivity is dramatically improved as well, demonstrating that D-PISEMO enables the measurement of individual dipolar couplings in 100% uniformly $^{13}C$ labeled peptides.

In the window-detected version of the experiment (W-PISEMO) diagrammed in Fig. 1C individual data points are acquired at the designated intervals of each WaHuHa cycle. Plotted as a function of time, these intensities constitute a dipolar free induction decay (dipolar FID) that can be subsequently Fourier transformed to yield a one-dimensional dipolar frequency spectrum. The evolution of the magnetization generated by the initial cross-polarization reflects only the $^{1}H$–$^{13}C$ heteronuclear dipole–dipole coupling, therefore this is a one-dimensional Shiftless NMR spectrum [10]. Since it contains all the dipolar coupling frequencies, it corresponds to the projection of the two-dimensional spectrum along the dipolar coupling frequency axis. As illustrated in Fig. 4, the projections of the two-dimensional spectra (Fig. 4A and C) are similar to the spectra obtained using the window-detected version of the same pulse sequences (Fig. 4B and D, respectively). Although many sites in the 100% uniformly $^{15}N$, $^{13}C$ labeled NAV single crystal contribute to the one-dimensional spectrum obtained with WD-PISEMO, the strong intensity and evidence of many individual splittings demonstrate that the experiment can deal with the network of $^{13}C$–$^{13}C$ homonuclear couplings. As Shiftless NMR spectra, the spectral resolution in Fig. 4B and D result entirely from the $^{13}C\alpha$ sites in different molecules in the unit cell having different $^{1}H$–$^{13}C\alpha$ heteronuclear dipolar coupling frequencies. Neither the $^{1}H$ nor the $^{13}C$ chemical shift interactions affect these spectra. Notably, it is feasible to obtain a high-resolution shiftless NMR spectrum even in situations where the sites have identical chemical shifts or the spectral resolution is limited by magnetic field inhomogeneities or instabilities. The feature illustrated here is that the one-dimensional projection derived from a two-dimensional experiment (Fig. 4A and C) can be replicated (Fig 4BD) in an experiment with reduced dimensionality. The windowed versions of D-PISEMO (Fig. 1B) can also be used as building blocks for more complex multidimensional experiments, in particular new classes of Shiftless NMR experiments.

To demonstrate applicability to a 100% uniformly $^{13}C$ labeled residues in a protein, the NMR spectrum in Fig. 5B is a slice taken

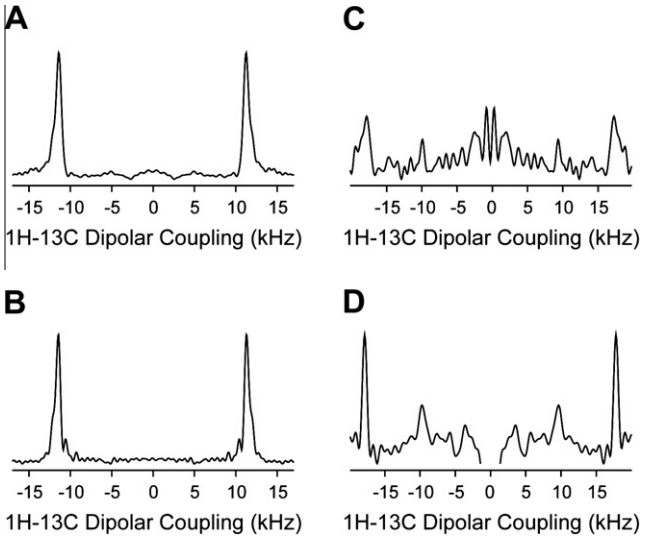


**Fig. 3.** One-dimensional slices along the $^{1}H$–$^{13}C$ dipolar coupling frequency dimension taken from the two-dimensional spectra displayed in Fig. 2. They correspond to a selected $^{1}H$–$^{13}C\alpha$ dipolar coupling. A and B are associated with the resolved peak marked with an arrow in Fig. 2A, C and D are associated with the partially resolved $^{13}C\alpha$ peak at 75 ppm marked with an arrow in Fig. 2D.

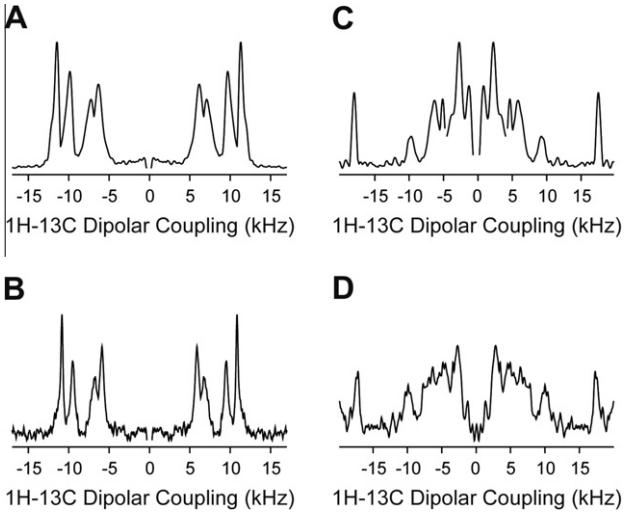


**Fig. 4.** One-dimensional $^{1}H$–$^{13}C$ dipolar coupling spectra that provide comparisons between the window-detected versions of the experiments and the projections of two-dimensional spectra shown in Fig. 2A and C are projections of two-dimensional spectra. B and D are window-detected one-dimensional spectra. A and B were obtained from a $^{15}N$, $^{13}C\alpha$ N-acetyl leucine (NAL) single crystal. C and D *were obtained* from a 100% uniformly $^{15}N$, $^{13}C$ labeled N-acetyl valine (NAV) single crystal. uniformly $^{15}N$, $^{13}C$ NAV single crystal.

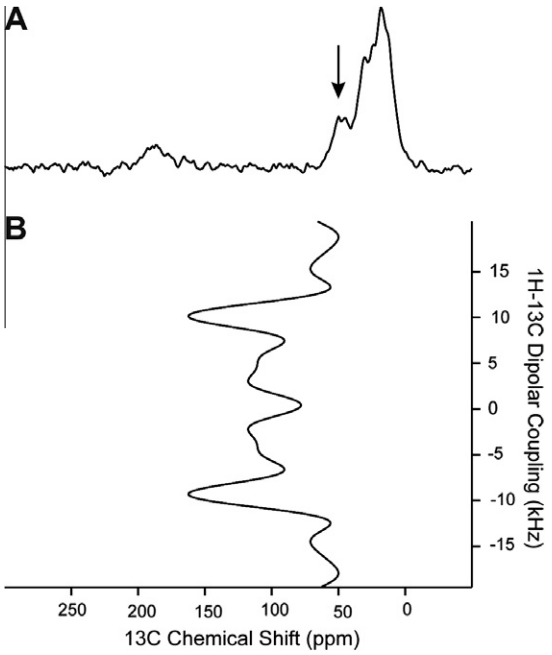


**Fig. 5.** (A) One-dimensional 13C chemical shift spectrum. B. One-dimensional $^{1}H$–$^{13}C\alpha$ dipolar coupling slice taken from a two-dimensional D-PISEMO spectrum. The spectra were obtained from the coat protein labeled 100% uniformly at its two leucine residues in fd bacteriophage magnetically aligned at 65 °C. The slice of the peak marked by the arrow (50 ppm) corresponds to a $^{13}C\alpha$ resonance. The two-dimensional NMR spectrum was acquired with 128 scans, 12 $t_1$ points, and 512 $t_2$ points. The dwell time was 36 μs and 20 μs for $t_1$ and $t_2$ dimensions, respectively. The cross-polarization time was 1 ms and the recycle delay was 6 s. The experimental data were zero filled to 512 and 1024 data points in $t_1$ and $t_2$ dimensions and were multiplied by a sine bell window function prior to Fourier transformation.

from a two-dimensional spectrum obtained with D-PISEMO. The sample is fd bacteriophage that is aligned by the magnetic field of the NMR spectrometer. The coat protein contains uniformly $^{13}C$ labeled leucine residues. The doublet in Fig. 5B is from the $^{1}H$–$^{13}C$ dipolar coupling associated with the leucine residue whose $^{13}C\alpha$ resonance is marked by the arrow in Fig. 5A.

## 3. Discussion

Separated local field spectroscopy is a particularly powerful experiment because it provides direct measurements of heteronuclear dipolar couplings associated with individual atomic sites in molecules as complex as proteins. When the $^{1}H$ and dilute spin, either $^{13}C$ or $^{15}N$, are directly bonded with fixed internuclear distances, then the frequencies of the dipolar couplings provide strong orientational constraints as input for structure calculations. The orientationally dependent chemical shift of each resonance provides complementary constraints for structure determination. Notably, in this type of spectroscopy, spectral resolution results from differences in orientations rather than chemical environments.

The combination of many $^{13}C$–$^{13}C$ dipole–dipole couplings in tight networks, the wide frequency range for isotropic chemical shift, and the wide frequency spans for carbonyl and aromatic carbon chemical shift anisotropy combine to make $^{1}H/^{13}C/^{15}N$ triple-resonance experiments challenging.

For the purpose of directly observing heteronuclear dipolar couplings, the experiments are limited to windowed or semi-windowless multiple-pulse sequences, which eliminate the use of Lee-Goldburg derived procedures. In general higher $B_1$ fields provide better decoupling, however, they could result in some problems for the windowed detection experiments. For example, decoupling with <50 kHz $B_1$ provides a 6.4 μs window for detection, but taking the delays of receiver and probe ringing into account, only 3.8 μs are available for signal acquisition. A larger $B_1$ field would result in a shorter window for detection, and with our current instrumentation a 70 kHz $B_1$ field is the limit for windowed detection.

In summary, the feasibility of simultaneously applying homonuclear dipolar coupling to the $^{1}H$ and $^{13}C$ nuclei to reveal individual dipolar couplings associated with single resonances has been demonstrated. The use of D-PISEMO provides substantial improvements in both resolution and sensitivity by incorporating homonuclear $^{13}C$–$^{13}C$ decoupling into the experiment. It can be performed as a conventional two-dimensional experiment, or with windowed detection as a one-dimensional experiment that offers flexibility for Shiftless and other multidimensional triple-resonance experiments on peptides and proteins. The use of 100% uniformly $^{15}N$, $^{13}C$ labeled proteins offers spectroscopic access to essentially all sites, and variations of the pulse sequences described here offer the potential for systematic assignment schemes and complete structure determinations that include the side chains in OS solid-state NMR.

## 4. Methods

### 4.1. NMR spectroscopy

The NMR experiments were performed on a Varian Inova spectrometer with $^{1}H$, $^{13}C$, and $^{15}N$ frequencies of 500.125 MHz, 125.76 MHz, and 50.68 MHz, respectively. In all experiments, the measured $B_1$ field was 50 kHz for the $^{1}H$ and $^{13}C$ channels, and 30 kHz for the $^{15}N$ channel. The $^{1}H$ chemical shift frequencies were referenced to the water as 4.7 ppm (25 °C). The $^{13}C$ chemical shift frequencies were referenced to the $^{13}CH_2$ resonance of adamantane as 38.47 ppm and the $^{15}N$ chemical shift frequencies were referenced to a $^{15}N$ labeled ammonium sulfate as 26.8 ppm, all as external references.

The windows between the multiple pulses can be utilized for signal acquisitions, and it is possible to acquire multiple sample points within each window. However, in these early experiments the observed signal-to-noise ratios are limited by practical aspects of optimizing analog and digital filters for windowed detection in multiple-pulse sequences. The numbers shown in Fig. 1C and D represent the timing of the data acquisitions in the windows, and the delay between the last pulse and acquisition is 2.6 μs which is limited by probe ringing. Two free induction decays (FIDs) were acquired in each window-detected experiment. The sample points acquired in the first and the third windows are taken as the data points in the first FID, and these points correspond to the odd and even $t_1$ dwells in PISEMO or D-PISEMO experiments. Similarly, the second FID is constituted from the sample points obtained in the second and the fourth windows. Because of the change in effective $B_1$ field, the two FIDs are added together after applying a 45° phase correction to the second FID. This results in an increase in the signal-to-noise ratio of approximately 20%. The scaling factors of W-PISEMO and WD-PISEMO are the same as those observed for PISEMO and D-PISEMO (0.67).

### 4.2. Triple-resonance NMR probe

A home-built triple-resonance probe was constructed specifically for these experiments using design principles consistent with applications to lossy biological samples [27]. It has an outer coil that is a modified Alderman-Grant Coil (MAGC), which operates at the proton ($^{1}H$) tuning frequency, and an inner solenoid coil that generates an orthogonal $B_1$ field. A similar double-resonance probe utilizing MAGC and solenoid coils has been previously described [28], and the probe described here is an extension of this design

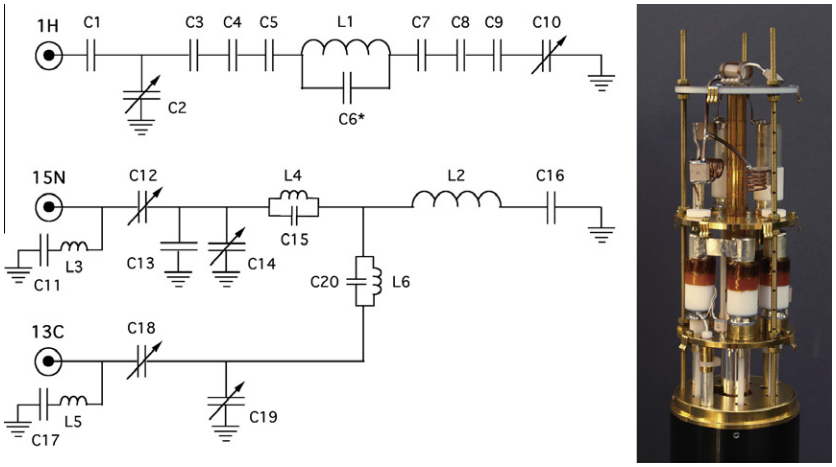


**Fig. 6.** Right: Photograph of the triple-resonance probe used in these experiments. Left: Circuit diagram for the triple-resonance MAGC probe pictured. L1 represents the outer 9 mm ID modified Alderman-Grant Coil and L2 is the seven-turn 5 mm ID inner solenoid coil. The values of the capacitors are: C1 = 2.7 pF, C3 = 6.8 pF, C4 = 6.8 pF, C5 = 6.8 pF, C7 = 12 pF, C8 = 12 pF, C9 = 12 pF, C11 = 6.8 pF, C13 = 33 pF, C15 = 12 pF, C16 = 56 pF, C17 = 6.8 pF, C20 = 56 pF. The capacitance C6* is 8.19 pF total integrated into the MAGC and consists of three parallel strings of four series ceramic chip capacitors. Capacitors C2, C10, C12, C14, C18 and C19 are variable capacitors with a range of 1–10 pF. Inductors L4 and L6 are eight turn and five turn 8 mm coils respectively.

with the incorporation of a third channel. In this triple resonance version of the probe, the inner 5 mm ID solenoid coil is double-tuned to the $^{15}N$ and $^{13}C$ frequencies, while the $^{1}H$ outer MAGC is as described previously [28]. The resulting cross-coil probe pictured in Fig. 6 offers several advantages over a more traditional modified Cross-Waugh circuit [29], in which a single solenoid sample coil is triply tuned, as used in our previous studies [30] and designs from other laboratories [31,32]. The main advantage of the MAGC is the dramatically reduced radio frequency (RF) heating that results from the low inductance of the MAGC. The low voltage drop across the leads of the coil significantly decreases the scalar electric field across the sample volume, which is the principal mechanism of sample heating during high frequency RF irradiation. Furthermore, the low inductance and relatively low filling factor ensure that the MAGC $^{1}H$ tuning frequency and resonance $Q$ factor are not significantly altered by the introduction of high dielectric, lossy biological samples that are extensively hydrated, such as the bacteriophage particles in aqueous solution in Fig. 5. The separation of the $^{1}H$ tuning circuit and coil assembly from the low frequency coil and circuit enables the choice of a solenoid inner sample coil of optimal inductance and filling factor for the $^{13}C$ and $^{15}N$ frequencies. A seven turn solenoid coil provides optimal inductance of the inner coil, and along with the simplified double resonance inner coil tuning circuit, we were able to obtain a significant increase in sensitivity compared to similarly constructed Cross-Waugh style single solenoid coil probes, which typically utilized a five or six turn 5 mm ID coil to ensure adequate $^{1}H$ performance in a triple tuned configuration. The $^{15}N$ and $^{13}C$ channels of the probe are isolated using a pair of band stop filters containing a significant amount of inductance (L4 and L6 in Fig. 6). This provides a durable double-tuned inner coil circuit that can withstand high power irradiation on one of the low frequency channels while observing the other. The probe performance is summarized in Table 1. The disadvantage of this design is that the low inductance and reduced filling factor of the outer MAGC make it rather insensitive for direct proton observation. This is not an issue in the class of experiments described in this article, since they are focused on direct $^{13}C$ detection.

**Table 1**
Summary of probe performance.

| Channel | Nutation frequency (kHz) | RF power (W) | RF homogeneity (A810/A90 × 100%) |
|---|---|---|---|
| $^{1}H$ | 71 | 109 | 73 |
| $^{13}C$ | 55 | 99 | 70 |
| $^{15}N$ | 55 | 280 | 70 |

### 4.3. Samples

The preparation of uniformly $^{13}C$ leucine labeled fd bacteriophage for high resolution NMR spectroscopy followed previous methods [19]. The samples for the solid-state NMR experiments were 5-mm o.d. thin-wall glass tubes containing 180 μl of 50 mg/ml solutions of bacteriophage in 5 mM sodium borate buffer, pH 8.0. Under these conditions, the bacteriophage particles align with their long axis parallel to the direction of the applied magnetic field. All of the isotopically labeled compounds and media described in this article are from Cambridge Isotope Laboratories (www.isotope.com).

## Acknowledgments

This research was supported by Grants from the National Institutes of Health, and it utilized the Biomedical Technology Resource for NMR Molecular Imaging of Proteins at the University of California San Diego, which is supported by Grant P41EB002031.

## References

[1] M. Meselson, F. Stahl, The replication of DNA in Escherichia coli, Proc. Natl. Acad. Sci. USA 44 (1958) 671.
[2] T.A. Cross, J.A. DiVerdi, S.J. Opella, Strategy for nitrogen NMR analysis of biopolymers, J. Am. Chem. Soc. 104 (1982) 1759–1761.
[3] M. Ikura, L.E. Kay, A. Bax, A novel approach for sequential assignment of proton, carbon-13, and nitrogen-15 spectra of larger proteins: heteronuclear triple-resonance three-dimensional NMR spectroscopy. Application to calmodulin, Biochemistry 29 (1990) 4659–4667.
[4] A. McDermott, T. Polenova, A. Bockmann, K.W. Zilm, E.K. Paulsen, R.W. Martin, G.T. Montelione, Partial NMR assignments for uniformly (13C, 15N)-enriched BPTI in the solid state, J. Biomol. NMR 16 (2000) 209–219.
[5] D.M. Schneider, R. Tycko, S.J. Opella, High-resolution solid-state triple nuclear magnetic resonance measurement of 13C–15N dipole–dipole couplings, J. Magn. Reson. 73 (1987) 568–573.
[6] J.S. Waugh, Uncoupling of local field spectra in nuclear magnetic resonance. Determination of atomic positions in solids, Proc. Natl. Acad. Sci. USA 73 (1976) 1394–1397.
[7] Z. Gu, S.J. Opella, Three-dimensional 13C shift/1H–15N coupling/15N shift solid-state NMR correlation spectroscopy, J. Magn. Reson. 138 (1999) 193–198.

[8] N. Sinha, F.V. Filipp, L. Jairam, S.H. Park, J. Bradley, S.J. Opella, Tailoring 13C labeling for triple-resonance solid-state NMR experiments on aligned samples of proteins, Magn. Reson. Chem. 45 (2007) S107–115 (Suppl 1).
[9] C.H. Wu, S.J. Opella, Proton-detected separated local field spectroscopy, J. Magn. Reson. 190 (2008) 165–170.
[10] C.H. Wu, S.J. Opella, Shiftless nuclear magnetic resonance spectroscopy, J. Chem. Phys. 128 (2008) 052312.
[11] G. Pake, Nuclear resonance absorption in hydrated crystals: fine structure of the proton line, J. Chem. Phys. 16 (1948) 327–336.
[12] J.S. Waugh, L.M. Huber, U. Haeberlen, Approach to high-resolution NMR in solids, Phys. Rev. Lett. 20 (1968) 180–182.
[13] W.I. Goldburg, M. Lee, Nuclear magnetic resonance line arrowing by a rotating rf field, Phys. Rev. Lett. 11 (1963) 255–258.
[14] J.S. Waugh, Uncoupling of local field spectra in nuclear magnetic resonance. Determination of atomic position in solids, Proc. Natl. Acad. Sci. USA 73 (1976) 1394–1397.
[15] C. Wu, A. Ramamoorthy, S. Opella, High-resolution heteronuclear dipolar solid-state NMR spectroscopy, J. Magn. Reson. A109 (1994) 270–272.
[16] A.A. Nevzorov, S.J. Opella, Selective averaging for high-resolution solid-state NMR spectroscopy of aligned samples, J. Magn. Reson. 185 (2007) 59–70.
[17] S. Opella, J. Waugh, Two-dimensional 13 C NMR of highly oriented polyethylene, J. Chem. Phys. 66 (1977) 4919–4924.
[18] T.A. Cross, S.J. Opella, Protein structure by solid-state NMR, J. Am. Chem. Soc. 105 (1983) 306–308.
[19] A.C. Zeri, M.F. Mesleh, A.A. Nevzorov, S.J. Opella, Structure of the coat protein in fd filamentous bacteriophage particles determined by solid-state NMR spectroscopy, Proc. Natl. Acad. Sci. USA 100 (2003) 6458–6463.
[20] Z.T. Gu, S.J. Opella, Two- and three-dimensional 1H/13C PISEMA experiments and their application to backbone and side chain sites of amino acids and peptides, J. Magn. Reson. 140 (1999) 340–346.
[21] Y. Ishii, R. Tycko, Multidimensional heteronuclear correlation spectroscopy of a uniformly 15N- and 13C-labeled peptide crystal: toward spectral resolution, assignment, and structure determination of oriented molecules in solid-state NMR, J. Am. Chem. Soc. 122 (2000) 1443–1455.
[22] N. Sinha, C.V. Grant, K.S. Rotondi, L. Feduik-Rotondi, L.M. Gierasch, S.J. Opella, Peptides and the development of double- and triple-resonance solid-state NMR of aligned samples, J. Pept. Res. 65 (2005) 605–620.
[23] A. Pines, M. Gibby, J. Waugh, Proton enhanced NMR of dilute spins in solids, J. Chem. Phys. 59 (1973) 569–590.
[24] W. Rhim, D. Elleman, R. Vaughan, Analysis of multiple pulse NMR in solids, J. Chem. Phys. 59 (1973) 3740–3749.
[25] U. Haeberlen, J.S. Waugh, Coherent averaging effects in magnetic resonance, Phys. Rev. 175 (1968) 453–467.
[26] N. Sinha, C.V. Grant, S.H. Park, J.M. Brown, S.J. Opella, Triple resonance experiments for aligned sample solid-state NMR of (13)C and (15)N labeled proteins, J. Magn. Reson. 186 (2007) 51–64.
[27] C.V. Grant, C.H. Wu, S.J. Opella, Probes for high field solid-state NMR of lossy biological samples, J. Magn. Reson. 204 (2010) 180–188.
[28] C.V. Grant, Y. Yang, M. Glibowicka, C.H. Wu, S.H. Park, C.M. Deber, S.J. Opella, A modified Alderman-Grant coil makes possible an efficient cross-coil probe for high field solid-state NMR of lossy biological samples, J. Magn. Reson. 201 (2009) 87–92.
[29] V. Cross, R. Hester, J. Waugh, Single coil probe with transmission line tuning for nuclear magnetic double resonance, Rev. Sci. Instrum. 47 (1976) 1486.
[30] N. Sinha, C. Grant, C. Wu, A. De Angelis, S. Howell, S. Opella, SPINAL modulated decoupling in high field double-and triple-resonance solid-state NMR experiments on stationary samples, J. Magn. Reson. 177 (2005) 197–202.
[31] F.D. Doty, R.R. Inners, P.D. Ellis, A multinuclear double-tuned probe for applications with solids or liquids utilizing lumped tuning elements, J. Magn. Reson. 43 (1981) 399–416.
[32] R. Martin, E. Paulson, K. Zilm, Design of a triple resonance magic angle sample spinning probe for high field solid state nuclear magnetic resonance, Rev. Sci. Instrum. 74 (2003) 3045.